Discovery of human hexosaminidase inhibitors by *in situ* screening of a library of mono- and divalent pyrrolidine iminosugars

Valeria Pingitore [a,1], Macarena Martínez-Bailén [a,1], Ana T. Carmona [a,*], Zuzana Mészáros [b,c], Natalia Kulik [d], Kristýna Slámová [b], Vladimír Křen [b], Pavla Bojarová [b,*], Inmaculada Robina [a], Antonio J. Moreno-Vargas [a,*]

[a] *Departamento de Química Orgánica, Facultad de Química, Universidad de Sevilla, C/ Prof. García González, 1, 41012-Sevilla, Spain*
[b] *Laboratory of Biotransformation, Institute of Microbiology of the Czech Academy of Sciences, Vídeňská 1083, 14220 Prague 4, Czech Republic*
[c] *Faculty of Food and Biochemical Technology, University of Chemistry and Technology Prague, Technická 1903/3, CZ-16628 Praha 6, Czech Republic*
[d] *Laboratory of Structural Biology and Informatics, Institute of Microbiology of the Czech Academy of Sciences, Zámek 136, CZ-37333 Nové Hrady, Czech Republic*

ARTICLE INFO

ABSTRACT

Two libraries of mono- and dimeric pyrrolidine iminosugars were synthesized by CuAAC and (thio)urea-bond-forming reactions from the respective azido/aminohexylpyrrolidine iminosugar precursors. The resulting monomeric and dimeric compounds were screened for inhibition of β-*N*-acetylglucosaminidase from Jack beans, the plant ortholog of human lysosomal hexosaminidases. A selection of the best inhibitors of these libraries was then evaluated against human lysosomal β-*N*-acetylhexosaminidase B (hHexB) and human nucleocytoplasmic β-*N*-acetylglucosaminidase (hOGA). This evaluation identified a potent (nM) and selective monomeric inhibitor of hOGA (compound **7A**) that showed a 6770-fold higher affinity for this enzyme than for hHexB. The corresponding dimeric derivative (compound **9D**) further remarkably improved the selectivity in the inhibition of hOGA (2.7×10^4 times more selective for hOGA over hHexB) and the inhibition potency (by one order of magnitude). Docking studies were performed to explain the selectivity of inhibition observed in compound **7A**.

1. Introduction

β-*N*-Acetylhexosaminidases (EC 3.2.1.52) are a family of exoglycosidases able to catalyze the cleavage of terminal β-*N*-acetyl-D-glucosamine (β-D-GlcNAc) and β-*N*-acetyl-D-galactosamine (β-D-GalNAc) residues in oligosaccharides and glycoconjugates [1]. Human hexosaminidases are involved in a wide variety of vital biological processes related to metabolism, cell communication [2], cell proliferation [3], and inflammation [4]. The GH20 human β-*N*-acetylhexosaminidases (hHex) [5] and the GH84 human β-*N*-acetylglucosaminidase (*O*-GlcNAcase, hOGA) [6] are of particular interest due to their potential as pharmacological targets for drug development. GH20 human lysosomal β-*N*-acetylhexosaminidases are dimeric enzymes composed of two subunits, α and β, which have approximately 60% identity in their amino acid sequence. These subunits are encoded by the genes *HEXA* and *HEXB* and are assembled to yield three enzyme isoforms: HexA (αβ), HexB (ββ) and HexS (αα) [1]. Mutations in the *HEXA* and *HEXB* genes lead to a

defect in these enzymes, causing the lysosomal storage diseases (LSDs) known as Tay-Sachs and Sandhoff, respectively. They stem from the accumulation of GM2 ganglioside in the lysosomes and are fatal neurodegenerative disorders [7]. Pharmacological chaperone therapy (PCT) is a novel therapeutic strategy for some LSDs and involves the use of small molecules that facilitate protein folding and trafficking to the lysosomes, preventing their early degradation. It has been reported that competitive glycosidase inhibitors can act as pharmacological chaperones [8]. This strategy has been studied *in vitro* for Fabry, Gaucher, GM1-gangliosidosis, Tay-Sachs, and Sandhoff diseases, all of which are LSDs [9,10]. In addition, HexA and HexB occur in an appreciable amount in the synovial fluid in patients with osteoarthritis [11]. The inhibition of these hexosaminidases can be considered as a strategy to prevent cartilage matrix degradation (chondroprotective activity), which represents a new strategy in the therapy of osteoarthritis [12]. hOGA catalyzes the cleavage of *O*-linked β-*N*-acetylglucosamine (*O*-GlcNAc) from serine or threonine residues in nucleocytoplasmic proteins [13]. Reverse

O-GlcNAcylation is catalyzed by *O*-GlcNAc transferase (OGT). Dysregulation of this deglycosylation/glycosylation cycle has been associated with *O*-GlcNAc-related diseases such as Alzheimer's [14] and cancer [15]. Although lysosomal hexosaminidases (HexA and HexB) and OGA belong to different CAZy families (GH20 and GH84, respectively), and are located in different cellular compartments, they are all GlcNAc-cleaving enzymes. Therefore, inhibitors of hHexA/B frequently also inhibit hOGA. Due to the diversity of biological activities of all these enzymes, the search for selective inhibitors for potential therapeutic applications is required.

Iminosugars are carbohydrate mimics that have been extensively studied in the development of glycosidase inhibitors. The generation and *in situ* biological screening of a library of compounds is a strategy widely used in drug discovery and has been applied successfully in the field of glycosidase inhibition. The main advantage of the strategy is the rapid identification of a bioactive compound with improved inhibitory properties, without the need to isolate individual compounds. This strategy has been explored in our research group for the development of potent inhibitors of α-mannosidases [16], α-fucosidases [17], β-glucosidases, and α-galactosidases [18]. We also reported for the first time the combination of click chemistry followed by *in situ* screening for the rapid discovery of potent divalent glycosidase inhibitors [19]. The multivalent approach was extensively studied in the field of carbohydrate-protein interactions and is based on the observation that the incorporation of multiple copies of a carbohydrate ligand into an appropriate platform increases the affinity of the resulting multimeric compound compared to the monomeric ligand [20]. Although the search for multivalent glycosidase inhibitors has been intense in the last ten years [21], the success of this strategy is limited to a few glycosidases. Among them, Jack bean α-mannosidase is one of the most susceptible to the multimeric presentations of inhibitors, with the multivalent inhibitor showing affinity enhancements of up to five orders of magnitude compared to the corresponding monovalent inhibitor [22]. Other interesting results using the multivalent strategy have been obtained with carbohydrate-active enzymes such as Golgi α-mannosidase II [23], yeast maltase [24] and *N*-acetylgalactosamine-6-sulfatase (GALNS) [25]. Our research group has recently reported the first example of a remarkable multivalent effect in the inhibition of human lysosomal α-galactosidase A, a homodimeric enzyme with allosteric binding pockets close to the active sites [26]. A wide range of monomeric inhibitors was described for hexosaminidases [27]; however, there is only one report on multivalent inhibitors of this enzyme recently described by Bleriot and coworkers [28]. The authors reported that the divalent presentation of a micromolar monomeric HexAB inhibitor resulted in a divalent structure that showed a 262-fold stronger inhibition and a better HexAB/OGA selectivity than the monovalent precursor.

The pyrrolidine iminosugar **1** is known to be a potent human β-*N*-acetylhexosaminidase inhibitor ($K_i = 40$ nM, human placenta) [12]. The NHAc moiety of **1** plays a crucial role in the hexosaminidase active site. Indeed, the substitution of the acetyl group by other larger substituents (derivatives **2**) always resulted in a dramatic decrease in the inhibitory activity of the resulting inhibitors [29], whereas the incorporation of an aminoalkyl group (compounds **3**) at the endocyclic nitrogen was not detrimental to inhibition. The amino group of the exocyclic chain proved to be important for the interaction with the enzyme, as the elimination of this group significantly decreased the inhibitory potency of the resulting inhibitors (compounds **4**) [30] (see Fig. 1).

We report here the synthesis of derivatives **3b** and **5** (Scheme 1) taking advantage of the fact that the amino or azido group in the alkyl chain can be useful functional groups for the generation of compound libraries using standard click reactions (CuAAC and (thio)urea-bond-forming reactions). These libraries were screened *in situ* against commercially available β-*N*-acetylglucosaminidase from Jack beans (JbGlcNAcase), which belongs to the GH20 family and is considered as a plant ortholog of human lysosomal hexosaminidases [31]. This methodology was also applied to the generation of a small library of dimeric hexosaminidase inhibitors. The best monomeric and dimeric inhibitors were evaluated using the human hexosaminidases hHexB and hOGA.

2. Results and discussion

We initially focused on the preparation and structure–activity evaluation of various libraries of monomeric compounds based on five-membered iminosugars. With this goal in mind, we performed the synthesis of the new hydroxylated azidohexylpyrrolidine **5** and the known hydroxylated aminohexylpyrrolidine **3b** [30] (see Supplementary data for details). Both pyrrolidine derivatives contain adequate functionality for the incorporation of different substituents through a click reaction in parallel synthesis. **Sub-library I** was generated by parallel CuAAC reactions. Each compound of the sub-library was formed by reaction of azidohexylpyrrolidine **5** (1.0 equiv.) with a commercial alkyne (2.4 equiv.) in the presence of CuSO$_4$·5H$_2$O (0.14 equiv.), sodium ascorbate (0.44 equiv.), and *t*-BuOH/H$_2$O as solvent (Scheme 1). In parallel, aminohexylpyrrolidine **3b** (1.2 equiv.) was reacted with 19 commercial iso(thio)cyanates (1.0 equiv.) for the generation of **sub-library II**, using DMSO as solvent. TLC and mass spectrometry (ESI-MS) were used to confirm the completion of each reaction (see Supplementary data). In **sub-library II**, a slight excess of aminohexylpyrrolidine **3b** was used to avoid the presence of iso(thio)cyanates in the final crude reaction mixtures that could react with the enzyme in the subsequent activity screening.

The crude reaction products of the 39-membered library (**sub-libraries I** and **II**) were diluted in water and tested *in situ* against JbGlcNAcase at a concentration of 0.25 μM (assuming complete conversion of **3b** and **5** to derivatives **6a-t** and **7A-S** in the reaction crudes) (see Fig. 2). The evaluation of azidohexylpyrrolidine **5** and aminohexylpyrrolidine **3b** against this enzyme showed that **5** is a weak inhibitor at the concentration used in this experiment (32% inhibition at 0.25 μM), whereas amine **3b** exhibited a stronger inhibition (71% at 0.25 μM). Thus, the excess of amine **3b** (0.2 equiv. excess) in generating the **sub-library II** should be taken into account in a direct comparison of the inhibitor potency of triazoles *vs.* (thio)ureas. Most triazoles (**6a-6t**) significantly improved the inhibition potency of the starting azide **5**. In the case of (thio)ureas, only some members of the library (**7A, 7B, 7E, 7H, 7J,** and **7Q**) slightly improved the inhibitory power of the parent aminohexyl pyrrolidine **3b**. For the other members, except for **7D, 7R**, and **7S**, the inhibition potency of the resulting (thio)ureas was similar to that of the precursor amine **3b**. In general, no significant differences in inhibition were observed depending on the aromatic/aliphatic nature of the moiety linked to the triazole/(thio)urea, except for triazoles **6e** and
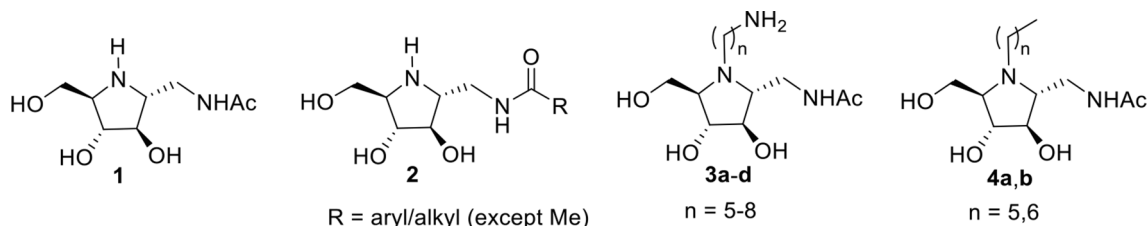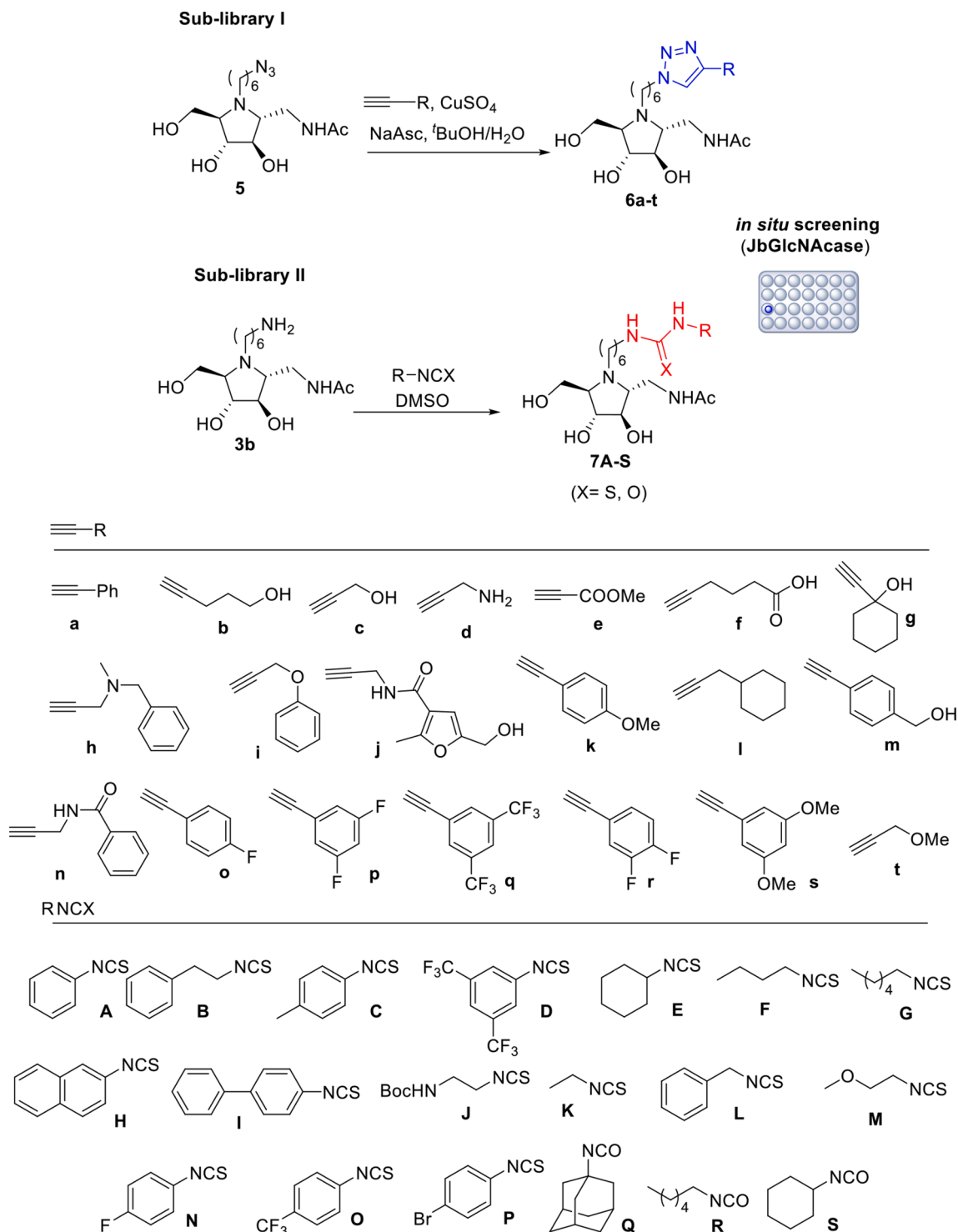

Fig. 1. Structure of the potent hexosaminidase inhibitor **1** and its derivatives obtained by modification of the endocyclic and exocyclic nitrogen.

Sub-library I

in situ screening
(JbGlcNAcase)

Sub-library II

≡—R

R NCX

Scheme 1. Generation of a 39-membered library of pyrrolidine-iminosugars.

6t that clearly exhibited the lowest inhibition potency. In blank tests with CuAAC reagents (CuSO$_4$, NaAsc, *t*-BuOH/H$_2$O), alkynes **a-s**, and DMSO, no inhibition of JbGlcNAcase was observed at the concentrations used in the screening, indicating that the presence of these reagents in the crude products could not interfere in the biological evaluation of the libraries.

To perform a complete kinetic analysis and prove the validity of the method, the most efficient compound of each sub-library in terms of inhibitory activity (**6s** and **7A**) and the derivatives **6t** and **7D** that had shown the weakest affinity for the enzyme were selected. These compounds were conventionally prepared at a larger scale and purified as indicated in Scheme 2.

Inhibition by triazoles **6s** and **6t**, thioureas **7A** and **7D**, and precursors **3b** and **5** was studied with a panel of eleven commercial glycosidases (for a list, see the Experimental section) and two recombinantly produced human hexosaminidases, hHexB and hOGA. hHexB was produced in the yeast expression system of *Pichia pastoris* and purified from the culture medium by ion-exchange chromatography as described in our previous work [32]. Human OGA was expressed in *Escherichia coli* as a His$_6$-tagged protein and purified by metal affinity
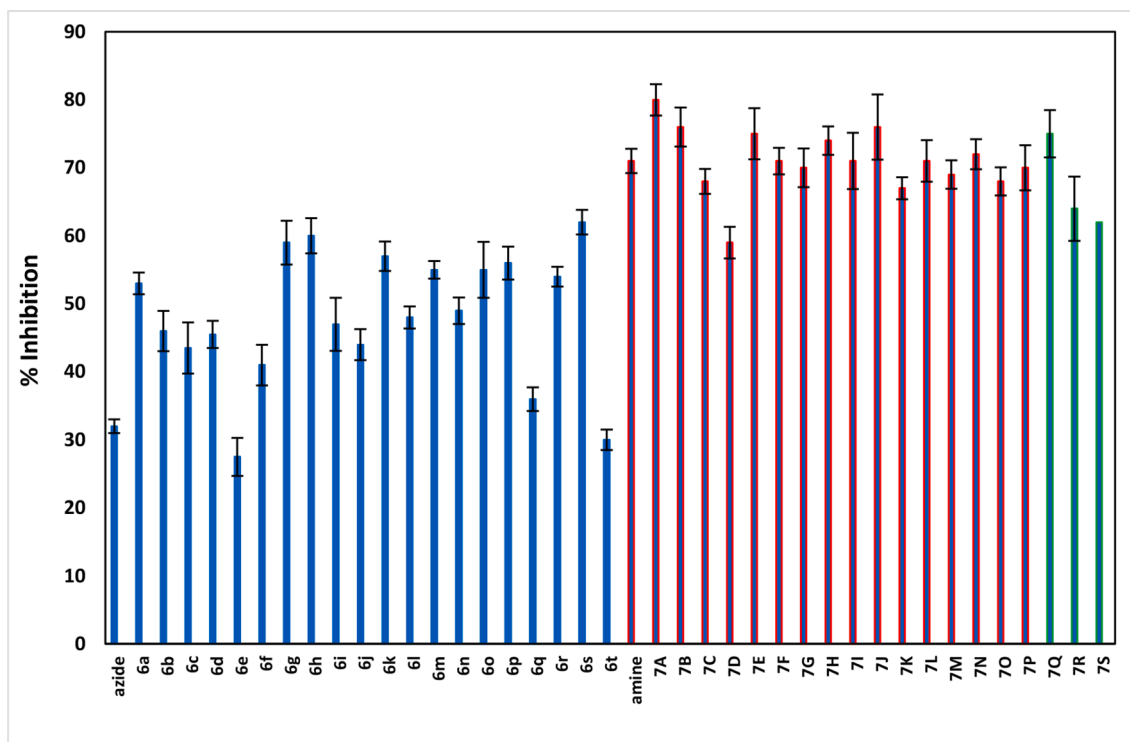
Fig. 2. Inhibitory activities toward JbGlcNAcase (pH 4, 37 °C) were measured for triazole derivatives **6a-t** (in blue), thiourea derivatives **7A-P** (in red), and urea derivatives **7Q-S** (in green) at 0.25 μM concentration in the well. Starting azide **5** at 0.25 μM (1.0 equiv. with respect to alkynes) and amine **3b** at 0.3 μM (1.2 equiv. with respect to iso(thio)cyanates) were also incorporated in the graph for comparison purposes. Each percentage of inhibition was determined in quadruplicate; the average value is given ± SEM ($n = 4$). The substrate used was 4-nitrophenyl β-*N*-acetyl-D-glucosaminide at a concentration of 0.83 mM ($K_M = 0.91$ mM, measured under screening conditions). (For interpretation of the references to colour in this figure legend, the reader is referred to the web version of this article.)
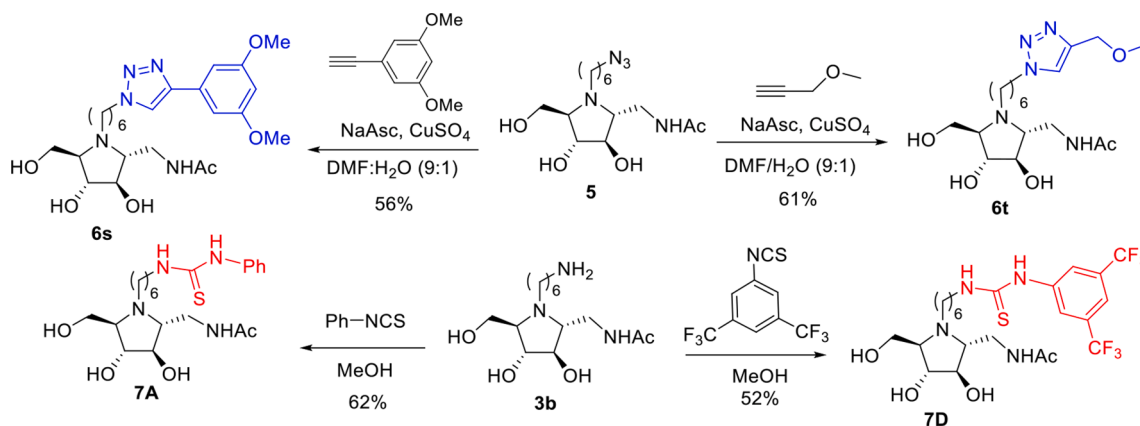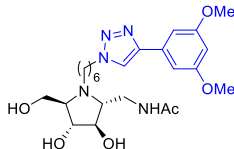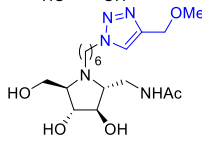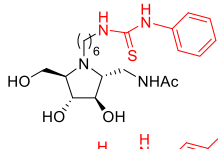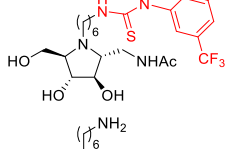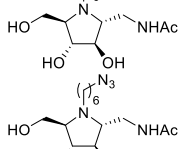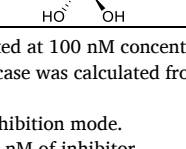

Scheme 2. Synthesis of monomeric triazole derivatives **6s** and **6t** and monomeric thioureas **7A** and **7D**.

chromatography. The results of the inhibition study are summarized in Table 1. All compounds were found not to inhibit other glycosidases from the panel than JbGlcNAcase, hHexB, and hOGA that were further tested. Regarding the inhibition of JbGlcNAcase, the IC$_{50}$ values were consistent with the results obtained previously in the *in situ* screening, with thiourea **7A** identified as the best inhibitor (IC$_{50}$ = 60 nM) and triazole **6t** as the weakest inhibitor (IC$_{50}$ = 246 nM). In the inhibition of human hexosaminidases, all the compounds showed strong inhibition (nM range) against hHexB and hOGA, except for thiourea **7A**, where a remarkable selectivity (hOGA *vs.* hHexB) was observed (Table 1). The inhibitory potency of the selected thioureas was significantly improved in the case of hOGA compared with the precursor amine **3b**. However, **3b** showed strong inhibition toward hHexB (59% at 100 nM) and its functionalization as thiourea did not significantly improve this

inhibition potency. On the other hand, triazole-derivatization of azide precursor **5** was an effective strategy to significantly increase the inhibitory potency toward both human and plant hexosaminidases. It is worth noting that the affinity of the selected compounds towards JbGlcNAcase correlates much more with that found for hOGA than with the observed in the inhibition of hHexB, although hHexB belongs to the same CAZy family as JbGlcNAcase. Interestingly, compounds **6s** and **7A** inhibited HexB in a non-competitive mode, while other compounds caused typical competitive inhibition of both enzymes. None of these compounds showed inhibition against the other ten commercial glyco-sidases tested at a concentration of 0.1 mM.

With these results in hand, we decided to apply this methodology to the search for dimeric inhibitors. A small library of divalent compounds was prepared using the linkage-based strategies and experimental

Table 1
Inhibitory potency of monovalent triazole derivatives and thioureas towards hexosaminidases.

Compound	Structure	K_i [nM][a] (IC_{50} [nM]) JbGlcNAcase	K_i [nM] hHexB	K_i [nM] hOGA	Selectivity for hOGA[d]
6s		56 ± 4 (108 ± 8)	221 ± 17[b]	154 ± 3.6	1.4
6t		127 ± 10 (246 ± 20)	92.3 ± 4.7	289 ± 9.7	0.32
7A		31 ± 3 (60 ± 6)	$322\,300 \pm 24\,000$[b]	47.6 ± 7.8	**6770**
7D		60 ± 5 (116 ± 10)	400 ± 8.8	50 ± 1.2	8
3b		80 ± 4 (155 ± 7)	59 %[c]	NI	–
5		327 ± 44 (632 ± 85)	NI	NI	–

NI: no inhibition detected at 100 nM concentration.
[a] The K_i on JbGlcNAcase was calculated from the measured IC_{50} value using the Cheng–Prusoff equation [$IC_{50} = K_i(1 + [S]/Km)$], assuming that the inhibition is competitive.
[b] Non-competitive inhibition mode.
[c] % Inhibition at 100 nM of inhibitor.
[d] Selectivity is defined as the ratio of K_is for HexB and for OGA.

procedures used for the monomers (Fig. 3) mixing 2.4–2.5 equiv. of azidohexylpyrrolidine **5** or aminohexylpyrrolidine **3b** and 1 equiv. of the corresponding dialkyne or diisothiocyanate. Several suitable divalent linkers with appropriate functionalization (diisothiocyanates **A-E** and dialkynes **a-e**, Scheme 3) were selected to connect two moieties of

3b or **5** (inhitopes). Aliphatic and aromatic linkers of different lengths were chosen to study the possible role of the linker in inhibition. TLC and mass spectrometry (ESI-MS) were used to confirm the completion of each parallel reaction (see Supplementary data).

Inhibitory activities toward JbGlcNAcase (pH 4, 37 °C) were
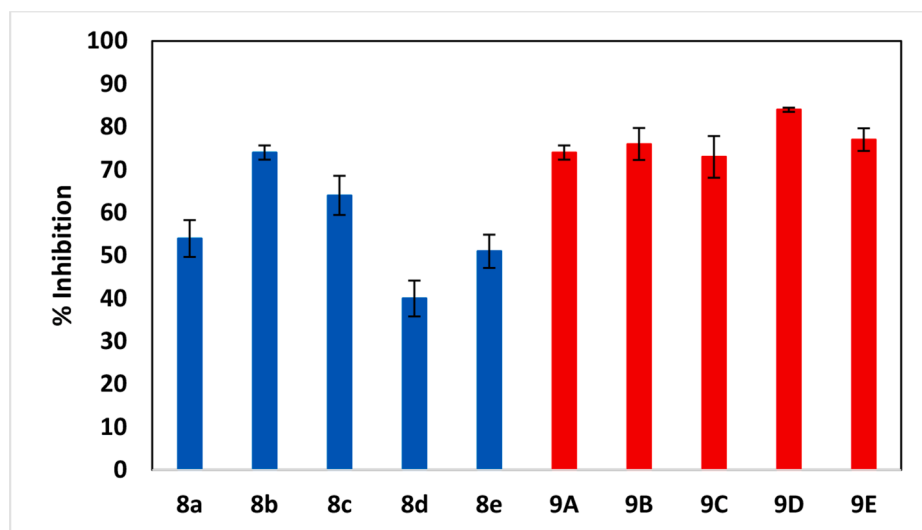
Fig. 3. Generation of a 10-membered library of dimeric pyrrolidine-iminosugars. Inhibitory activities towards JbGlcNAcase (pH 4, 37 °C) measured for dimeric triazole (in blue) and thiourea (in red) inhibitors at 75 nM concentration in the well. Each % of inhibition was determined in quadruplicate, the average value is given $\pm$ SEM ($n = 4$). 4-Nitrophenyl β-*N*-acetyl-ᴅ-glucosaminide at 0.83 mM concentration was used as substrate. (For interpretation of the references to colour in this figure legend, the reader is referred to the web version of this article.)
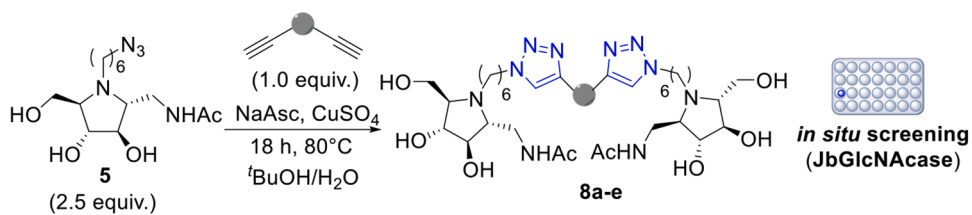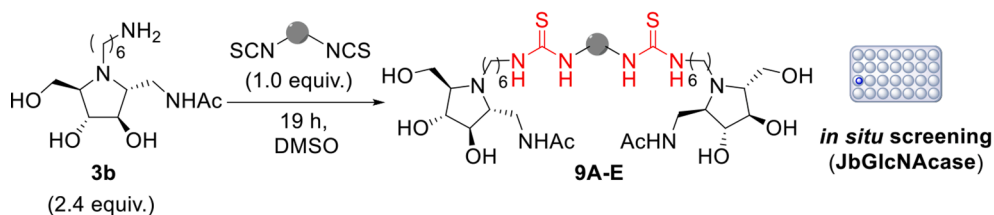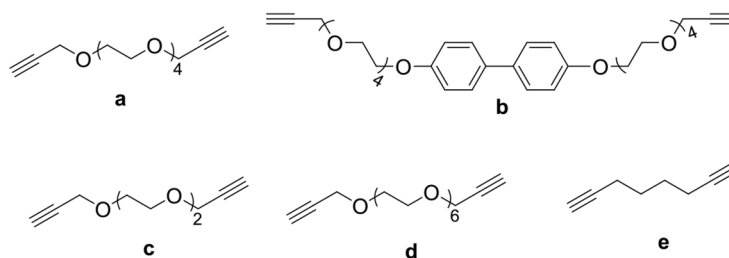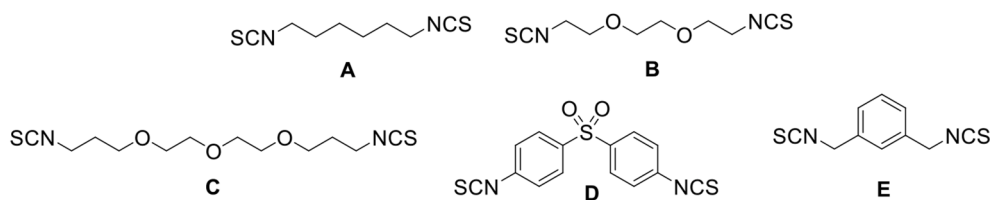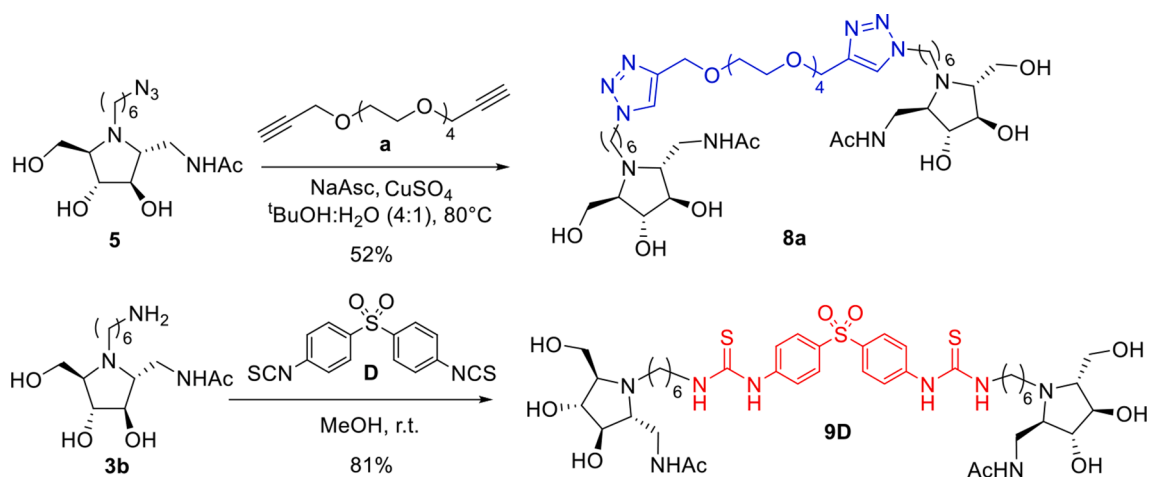
Scheme 3. Generation of a 10-membered library of dimeric pyrrolidine-iminosugars.

Scheme 4. Synthesis of dimers **8a** and **9D**.

measured for dimeric triazoles **8a-e** (in blue) and dimeric thioureas **9A-E** (in red). The *in situ* biological screening was performed at a lower concentration (75 nM) than for the monomeric analogs (250 nM) since a higher inhibitory activity was expected for the dimers compared to the monomers. In this case, the excess of pyrrolidine **3b** in the experiments leading to thioureas **9A-9E** did not affect the inhibition (%) of the resulting dimers as **3b** was a weak inhibitor of JbGlcNAcase at 75 nM (36% inhibition). Dithiourea derivatives **9A-E** proved to be slightly better inhibitors than ditriazoles **8a-e** as previously observed with the corresponding monomeric counterparts. Triazoles were more sensitive than thioureas to the nature of the linker, nevertheless, no significant differences in the inhibitory potency were observed.

Compound **9D** with the highest inhibitory potency (84% inhibition) and derivative **8a** were synthesized by conventional methods and purified at a larger scale (Scheme 4). Both compounds were again evaluated against a panel of eleven commercial glycosidases (for a list, see the Experimental section) and the two human hexosaminidases. Apart from the inhibition against the three hexosaminidases tested (Table 2), no inhibition of other glycosidases was observed with the dimer inhibitors at a concentration of 0.1 mM. The corresponding results are shown in Table 2. Compounds **8a** and **9D** exhibited a strong inhibition of JbGlcNAcase (IC$_{50}$ = 24 nM and 11 nM, respectively), as previously observed in the *in situ* screening. As for the inhibition of human hexosaminidases, dithiourea **9D** showed a much better inhibition profile than **8a**, being a stronger inhibitor of hOGA (K_i = 6.1 nM *vs.* 127 nM, respectively) and remarkably, much more selective. Compound **9D** exhibited a K_i = 168 μM for hHexB, whereas **8a** had a K_i = 88 nM. No significant multivalent effect was observed in the inhibition of any of the hexosaminidases by both dimers when the corresponding inhibition values were compared with those of the monomeric counterparts, triazole **6t** and thiourea **7A**, respectively. However, the divalent presentation of **7A** significantly improved selectivity in the inhibition of hOGA over hHexB by increasing the selectivity of inhibition for hOGA compared to hHexB from nearly 6800-fold in monomer **7A** to 27500-fold in the corresponding dimer **9D**.

The high selectivity observed in the inhibition of hOGA *vs.* hHexB by monomer **7A** and by its corresponding dimer **9D** resulted from their exceptionally low inhibitory potency toward hHexB compared, for example, with the structurally similar monomer **7D** (Table 1). We attempted to find an explanation for these observations by molecular docking of monomeric inhibitors **7A** and **7D** into the model structure of hHexB. The complete model of hHexB was built based on its known crystal structure (PDB ID: 1now [33] and 1o7a [34]) by loop modeling as described in [32]. The structures of inhibitors were modeled in YASARA [35] and docked into the active site of the crystal structures. Both inhibitors **7A** and **7D** could be docked with their iminosugar moiety within the active site of the enzyme (Fig. 4A). However, several other possible positions outside the active site were found for both **7A** and **7D**. The best-scored poses (in the active site and outside the active site) identified by the Glide SP algorithm [36] were saved and ranked by Glide XP [37]. The final MM-GBSA free energy of binding (ΔG) [38] and

Glide XP scores [37] for the best-minimized complexes (Fig. 4, and Supporting Information, Fig. S14) are listed in Table 3. Lower energies indicate better binding. The interactions and orientation of the iminosugar moiety of **7A** and **7D** docked into the active site of hHexB were similar for both inhibitors and resembled the interactions formed by the known inhibitor 2-acetamido-2-deoxy-D-glucono-1,5-lactone previously co-crystallized with human HexB (PDB ID: 1o7a [34]) – see Fig. 4C, D. The iminosugar moiety common for both **7A** and **7D** formed hydrogen bonds with the following active site residues of monomer A: Tyr450 and Asp354 with *N*-acetyl; catalytic Glu355 with the C-3 hydroxyl, Arg211 with the C-4 hydroxyl, Glu491 with the C-4 or C-6 hydroxyl groups (Fig. 4C, D). The only stable interaction with monomer B of hHexB could be formed by the C-6 hydroxyl and Tyr456 (Fig. 4D). The aliphatic chain of **7A** and **7D** was placed in a hydrophobic groove formed exclusively by residues of monomer A (Fig. 4A, B): the hydrophobic contacts were established with Leu453, the methylene group of Asp426, Trp424, and the aromatic ring of Tyr450. The hydrogen bonds formed by the carbonyl group of the backbone of Ala447 and the thiourea group of the inhibitor stabilized the position of the inhibitors closer to the enzyme (Fig. 4C, D). The phenyl group of **7A** formed only the hydrophobic interaction with the methylene groups of Lys462 and did not interact with Leu453. In contrast, the interaction of the 3,5-(trifluoromethyl) phenyl group of **7D** with the enzyme was more complex. The HexB surface close to fluorines of the docked **7D** was polarized (Fig. 4B) and the geometry of bound **7D** might allow the fluorine to form a halogen bond with the backbone oxygen of Leu453 (as identified by Protein-Ligand interaction profiler [39]) and a weak hydrogen bond with Lys462 (as identified by LigPlot [40]). To estimate the interaction energy between these residues and the inhibitors, we calculated the strength of interaction of **7D** or **7A** with Leu453 (backbone oxygen) and Lys462 (side-chain) using the QM method with Gaussian in the gas phase [41] (Supporting Information, Fig. S15). It showed that the interaction energy between **7D** and Leu453 backbone oxygen was not favorable for the binding of **7D** (Supporting Information, Table S1); therefore, we suspect that the halogen bond was not formed in this case. In contrast, the interaction of Lys462 with **7D** improved its binding by 9.12 kJ/mol compared with **7A** (Supporting Information, Figure S15). The docking revealed alternative binding sites outside the active site, which were different for **7A** and **7D** (Supporting Information, Fig. S14). The alternative binding site for **7A** is located next to the flexible loop 310–318. Remarkably, this loop is resolved only in the 1now [33] structure and is flexible in human HexB; hence the inhibitor could not frequently occupy this position. The free energy of binding of **7A** was comparable to its binding into the active site (Table 3). In contrast, **7D** was water-exposed in its alternative binding site and had a significantly higher binding score (Table 3). This observation supports the results of our kinetic studies, which showed that compound **7A** inhibits hHexB in a non-competitive mode. Furthermore, we conclude that **7D**, because it does not have the possibility of two favorable binding sites, competes more efficiently with the substrate in the active site of hHexB and has a higher inhibitory potency (lower K_i) for hHexB. This is fully consistent with our kinetic study showing the competitive mode of inhibition of **7D** with hHexB. In summary, we hypothesize that the presence of an energetically favorable alternative binding site for **7A** and the positive effect of the additional interaction of **7D** with the active site residue Lys462 (absent in **7A**) could explain the differences found in inhibition constants between **7A** and **7D**.

3. Conclusions

The combination of parallel synthesis *via* click reactions and *in situ* screening has enabled the identification of potent nanomolar iminosugar inhibitors of Jack bean β-*N*-acetylglucosaminidases. The method proved to be efficient in determining the best endocyclic nitrogen substituent(s) of a pyrrolidine iminosugar-based library for the most efficient inhibition of these enzymes. This methodology also proved to be

Table 2
Inhibitory potency of selected dimers towards hexosaminidases.

Compound	K_i [nM][a] (IC$_{50}$ [nM]) JbGlcNAcase	K_i [nM] hHexB	K_i [nM] hOGA	Selectivity for hOGA[b]
Dimer **8a**	12 ± 1 (24 ± 1)	88.0 ± 7.6	127 ± 10	0.69
Dimer **9D**	6 ± 1 (11 ± 2)	168 000 ± 12 300	6.1 ± 1.1	**27 500**

[a] The K_i on JbGlcNAcase was determined from the measured IC$_{50}$ value using the Cheng–Prusoff equation [IC$_{50}$ = K_i(1 + [S]/K_M)], assuming that the inhibition is competitive.

[b] Selectivity is defined as the ratio of K_is for hHexB and for hOGA. The inhibitory mode was competitive for both dimeric inhibitors tested.
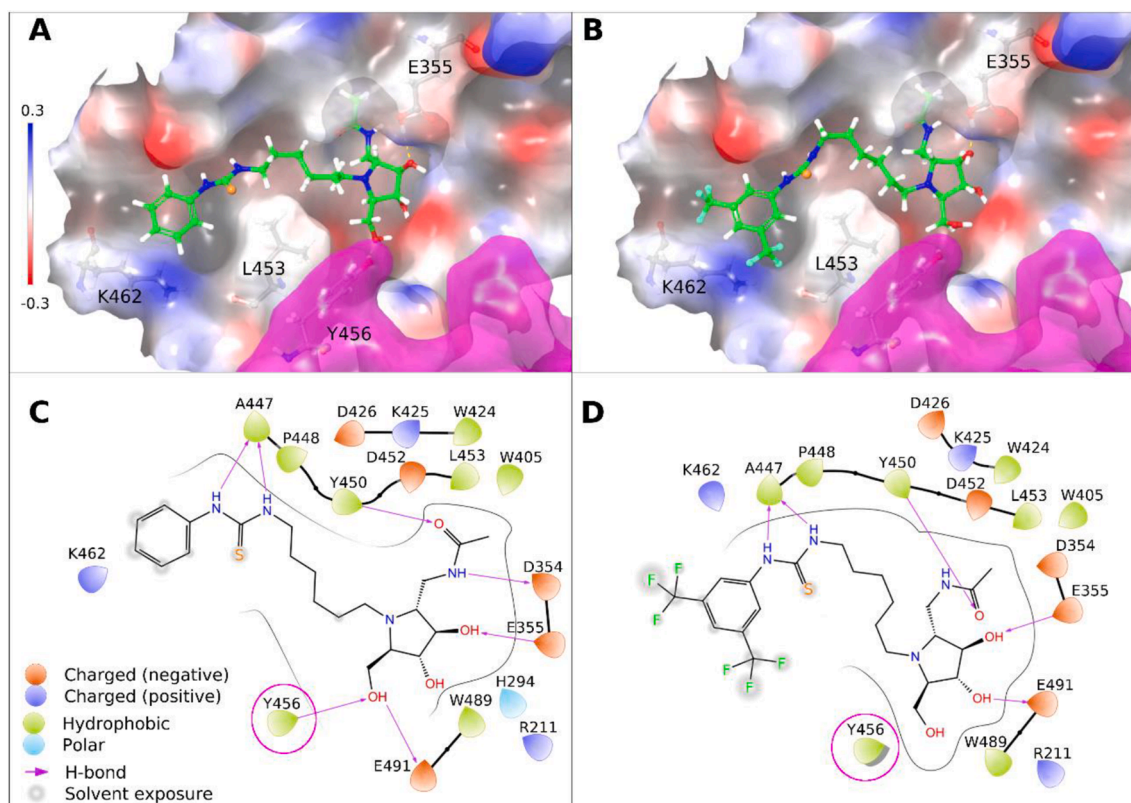
Fig. 4. Docked orientations of inhibitors in the hHexB active site (**A**, **C** for **7A**; **B**, **D** for **7D**). **A, B**. Amino acid residues of monomer A located within 8 Å of the docked inhibitors are represented by the accessible surface area colored according to the electrostatic potential (red - negatively charged, blue – positively charged). The inhibitors are shown in ball and stick representation: carbons in green, fluorines in light green, hydrogens in white, oxygens in red, nitrogens in blue, sulfur in orange. The position of the catalytic residue Glu355 and other important residues discussed (Lys462 and Leu453 of monomer A and Tyr456 of monomer B) are shown and marked. Monomer B is represented by the accessible surface area in magenta. **C, D**. Schematic representation of inhibitor interactions prepared using Schrödinger software. The amino acid residues within 3.5 Å from inhibitors are labeled in one-letter code. (For interpretation of the references to colour in this figure legend, the reader is referred to the web version of this article.)

Table 3
Binding analysis of inhibitors **7A** and **7D** to hHexB by molecular modeling.

Inhibitor	Binding site	ΔG (MM/GBSA calculation) [kJ/mol]	Glide XP score [kJ/mol]
7A	Active site	−278.7	−35.9
	Alternative site	−269.2	−24.7
7D	Active site	−259.9	−41.6
	Alternative site	−205.3	−19.6

efficient in the rapid screening for the best linker to design a potent dimeric hexosaminidase inhibitor. This preliminary activity screening allowed us to select the best candidates to be evaluated as inhibitors of two biomedically relevant human β-*N*-acetylhexosaminidases (GH20 hHexB and GH84 hOGA). This strategy enabled us to identify the monomeric thiourea-based inhibitor **7A** and especially its dimeric analog **9D**, which proved to be a nanomolar and remarkably selective inhibitor of hOGA (K_i = 6.1 nM for hOGA *vs* K_i = 168 μM for hHexB).

4. Experimental section

4.1. Chemistry. General methods

Optical rotations were measured in a Jasco P-2000 in a 1.0 cm or 1.0 dm tube (Na, λ 598 nm). ^{1}H- and ^{13}C NMR spectra were recorded with a Bruker AMX300 spectrometer for solutions in CDCl$_3$ and CD$_3$OD. δ are given in ppm and *J* in Hz. Chemical shifts are calibrated using residual solvent signals (CDCl$_3$: δ(H) = 7.26, δ(C) = 77.16; CD$_3$OD: δ(H) = 3.31,

δ(C) = 49.00). *J* are assigned and not repeated. All the assignments were confirmed by 2D spectra (COSY and HSCQ). High-resolution mass spectra were recorded on a Q-Exactive spectrometer. TLC was performed on silica gel 60 F$_{254}$ (Merck), with detection by UV light charring with *p*-anisaldehyde, KMnO$_4$, ninhydrin, phosphomolybdic acid or with reagent [(NH$_4$)$_6$MoO$_4$, Ce(SO$_4$)$_2$, H$_2$SO$_4$, H$_2$O]. Silica gel 60 (Merck, 40–60 and 63–200 μm) was used for preparative chromatography.

4.2. HexB and OGA (experimental details for the enzyme expression)

Human HexB was expressed extracellularly in the methylotrophic yeast *Pichia pastoris* KM71H and purified from its culture media as described previously [32]. The gene of human OGA containing a His$_6$-tag was obtained as a kind gift from Prof. D. Vocadlo (SFU, Burnaby, Canada). hOGA was expressed intracellularly in *E. coli* BL21 (DE3) pLysS strain under the induction with 0.5 mM IPTG (isopropyl β-D-thio-galactoside, Merck, DE). After 16 h of cultivation at 25 °C, cells were harvested by centrifugation and lysed in a freshly prepared lysis buffer for 45 min at 37 °C (250 μL Triton X-100, 200 μL 1 M MgCl$_2$, 2.5 mL 1 M NaCl, 50 μg lysozyme, 500 μL PMSF (phenylmethanesulfonyl fluoride, Merck, DE); all dissolved in binding buffer (20 mM Na$_2$HPO$_4$, 0.5 M NaCl, 20 mM imidazole, pH 7.4) to a total volume of 50 mL). The cells were then disrupted by sonication (6 × 1 min) and cell debris was removed by centrifugation. The supernatant was diluted 1:2 by the binding buffer and loaded onto a 5 mL HisTrap column (GE Healthcare, US) connected to the Äkta Purifier protein chromatography system (GE Healthcare, US). The proteins bound to the column were eluted by the elution buffer (20 mM Na$_2$HPO$_4$, 0.5 M NaCl, 500 mM imidazole, pH

7.4) and the hOGA containing fractions were collected, diluted with 100 mM Tris/HCl + 100 mM NaCl buffer pH 7.4 and concentrated using Amicon Ultra Centrifugal Filters (Merck, DE). Both hHexB and hOGA were stored at 4 °C, where their activity remained stable for several months.

4.3. Inhibition studies with commercial enzymes

A panel of 11 commercial glycosidases (α-L-fucosidase from *Homo sapiens*, α-galactosidase from coffee beans, β-galactosidases from *E. coli* and *Aspergillus oryzae*, α-glucosidases from yeast and rice, amyloglucosidase from *A. niger*, β-glucosidase from almonds, α-mannosidases from Jack beans, β-mannosidase from *Helix pomatia*, and β-*N*-acetylglucosaminidase from Jack beans (JbGlcNAcase) was tested with prepared inhibitors. These enzymes were purchased from Sigma-Aldrich or Megazyme. The inhibitory activity (% inhibition) towards the corresponding glycosidase was determined in quadruplicate in the presence of the assumed concentration of the inhibitor in the well, presuming 100% conversion. Each enzymatic assay (final volume 0.12 mL) contained 0.01–0.5 U/mL of the enzyme (with the previous calibration) and an aqueous solution of the corresponding *p*-nitrophenyl glycopyranoside (substrate) buffered to the optimal pH of the enzyme. Enzyme and inhibitor were pre-incubated at a constant temperature for 5 min, and the reaction was started by adding the substrate. After 20 min of incubation at 37 °C, the reaction was stopped by the addition of 0.1 mL of a pH 10 solution. The *p*-nitrophenolate formed was measured by visible absorption spectroscopy at 405 nm (Asys Expert 96 spectrophotometer). Under these conditions, the released *p*-nitrophenolate resulted in absorbances linear with both reaction time and concentration of the enzyme. The IC_{50} value (concentration of inhibitor required for 50% inhibition of enzyme activity) was determined from plots of % inhibition *versus* log [inhibitor concentration]. Each value in the graph is the average of four measurements.

4.4. Inhibition studies with human HexB and OGA

The enzyme activity was measured in a discontinuous spectrophotometric assay employing *p*NP-β-GlcNAc as substrate at a starting concentration of 2 mM. The reaction mixture was incubated in 50 mM citrate/phosphate buffer pH 7.0 (OGA) or 5.0 (HexB) for 10 min at 35 °C and 900 rpm. Then, the reaction (50 μL) was stopped by adding 0.1 M Na_2CO_3 (1 mL) and the concentration of released *p*-nitrophenol was determined spectrophotometrically at 420 nm. One unit of enzymatic activity corresponds to the amount of enzyme releasing 1 μmol of *p*-nitrophenol per minute under the above conditions. The kinetic and inhibitory parameters of human OGA (4.09 U/mg) and β-*N*-acetylhexosaminidase B (12.3 U/mg) were measured spectrophotometrically in a discontinuous assay using Tecan plate reader. From the reaction mixture (volume 300 μL), which contained the respective enzyme (OGA 20 μL; HexB 10 μL), *p*NP-β-GlcNAc as substrate with a concentration in the range of 0.1–2 mM and inhibitor **6s**, **6t**, **7A**, **7D**, **8a**, and **9D** at various concentrations (30 μL) in 50 mM citrate/phosphate buffer pH 7.0 (OGA) or 5.0 (HexB) at 35 °C and 900 rpm, samples (50 μL) were taken in 1-minute intervals into microplate wells containing 150 μL of 0.1 M Na_2CO_3 for enzyme inactivation and the resulting absorbance at 420 nm was measured. The inhibition constants (K_i) were calculated using GraphPad Prism (GraphPad, UK); all data were measured in three parallel experiments.

4.5. Docking studies with hHexB

Crystal structures of hHexB were downloaded from Protein Data-Bank [42]– PDB ID: 1now [33]; 1o7A [34]. Unresolved loops were modeled as described [32]. Inhibitor structures were built and optimized using the YASARA program [35].

Binding poses were searched using the GlideSP algorithm [36] by

flexible ligand docking in the active site of hHexB crystals (1now and 1o7a). Inhibitors for docking were sampled by LigPrep (part of Schrödinger software). The enzymes were prepared by protonation at pH 6. Incorrect atom names and bond orders were corrected and minimized in the OPLS-2003 force field by Protein Preparation Wizard. The catalytic residue Glu355 was modeled in the protonated state.

Several alternative poses of ligands identified by GlideSP were saved and scored using the GlideXP method [37]. The best-scored poses (one in the active site and one outside the active site) were selected for further analysis. The found positions of inhibitors were again optimized by short minimization in implicit VGSB water solvent in OPLS-2003 force field with fixed residues more than 0.5 nm away from the docked inhibitor. The final minimized complexes were again scored by GlideXP algorithm by rigid scoring in place. The results are shown in Table 3. In addition, the method MM-GBSA [38] was used to calculate the binding free energy ΔG; lower values indicate better binding:

$$\Delta G_{binding} = \Delta G_{complex,\ solvated} - (\Delta G_{receptor,\ solvated} + \Delta G_{ligand,\ solvated})$$

Interactions between inhibitors and enzymes were analyzed by Maestro (part of Schrödinger software), the Protein-Ligand Interaction Profiler [39], and LigPlot [40]. Additionally, the interactions determined between phenyl or 3,5-bis(trifluoromethyl)phenyl groups of inhibitors with HexB residues were further evaluated by the QM calculation. The QM calculation was run in a gas phase in Gaussian 09 [41] with DFT method with X3LYP functional [43] and cc-pVTZ basis sets, recommended for the correct treatment of halogen bonds [44]. The simplified systems and results of QM calculation are shown in the Supporting Information, Figs. S14, S15, and Table S1.

4.6. Generation of the monomeric sub-libraries I and II followed by in situ biological screening

Sub-library I: To a solution of 300 μL of the azidohexylpyrrolidine **5** (37.5 mM in *t*-BuOH:H₂O, 2:1) in an Eppendorf tube, we added 100 μL of a solution of the corresponding alkyne (**a-t**) (270 mM in *t*-BuOH) followed by 25 μL of a solution of sodium ascorbate (198 mM in H_2O) and 25 μL of a solution of $CuSO_4 \cdot 5H_2O$ (62 mM in H_2O). The final concentration of the azidohexyl pyrrolidine **5** in each Eppendorf tube was 25 mM. The resulting mixtures were shaken at 50 °C for 21 h and monitored for completion by TLC (EtOAc:MeOH, 3:1) and ESI-MS. Then, the reactions were diluted with water to the assumed concentration of pyrrolidine-triazole of 1.5 μM and placed in a 96-well microtiter plate to perform the enzymatic assays towards JbGlcNAcase. In the preliminary screening of the resulting crudes (**6a-6t**), the percentage of inhibition was determined at 0.25 μM of the corresponding pyrrolidine-triazole in each well (assuming quantitative conversion in the click reaction).

Sub-library II: To a solution of 250 μL of the aminohexylpyrrolidine **3b** (28 mM in DMSO) in an Eppendorf tube, we added 83 μL of a solution of the corresponding iso(thio)cyanates (**A-S**) (70 mM in DMSO). The final concentration of the iso(thio)cyanates (**A-S**) in each Eppendorf tube was 17.5 mM. The resulting mixtures were shaken at r.t. for 6 h and monitored for completion by TLC (EtOAc:cyclohexane, 1:1) and ESI-MS. Then, the reactions were diluted with water to the assumed concentration of pyrrolidine-(thio)urea of 1.5 μM and placed in a 96-well microtiter plate to perform the enzymatic assays toward JbGlcNAcase. In the preliminary screening of the resulting crude (**7A-7S**), the percentage of inhibition was determined at 0.25 μM of the corresponding pyrrolidine-(thio)urea in each well (assuming quantitative conversion in the click reaction).

4.7. Generation of the dimeric libraries followed by in situ biological screening

Dimeric triazoles: To a solution of 84 μL of the azidohexylpyrrolidine **5** (90 mM in *t*-BuOH) in an Eppendorf tube, we added 35

μL of a solution of the corresponding dialkyne (**a-e**) (86 mM in *t*-BuOH) followed by 15 μL of a solution of sodium ascorbate (200 mM in H_2O) and 14 μL of a solution of $CuSO_4 \cdot 5H_2O$ (60 mM in H_2O). The final concentration of the dialkynes (**a-e**) in each Eppendorf tube was 20 mM. The resulting mixtures were shaken at 80 °C for 18 h and monitored for completion by TLC (EtOAc:cyclohexane, 2:1) and ESI-MS. Then, the reactions were diluted with water to the assumed concentration of dimeric triazole of 450 nM and placed in a 96-well microtiter plate to perform the enzymatic assays towards JbGlcNAcase. In the preliminary screening of the resulting crude (**8a-8e**), the percentage of inhibition was determined at 75 nM of the corresponding dimeric compound in each well (assuming quantitative conversion in the click reaction).

Dimeric thioureas: To a solution of 100 μL of the amino-hexylpyrrolidine **3b** (90 mM in DMSO) in an Eppendorf tube, we added 88 μL of a solution of the corresponding diisothiocyanates (**A-E**) (43 mM in DMSO). The final concentration of the diisothiocyanates (**A-E**) in each Eppendorf tube was 20 mM. The resulting mixtures were shaken at r.t. for 19 h and monitored for completion by TLC (EtOAC:cyclohexane 1:2) and ESI-MS. Then, the reactions were diluted with water to the assumed concentration of dimeric thiourea of 450 nM and placed in a 96-well microtiter plate to perform the enzymatic assays towards JbGlcNA-case. In the preliminary screening of the resulting crude (**9A-9E**), the percentage of inhibition was determined at 75 nM of the corresponding dimeric compound in each well (assuming quantitative conversion in the click reaction).

4.8. Synthetic details for new compounds

(2R,3R,4R,5R)-2-Acetamidomethyl-1-(6-(4-(3,5-dimethoxyphenyl)-1H-1,2,3-triazol-1-yl)hexyl)-5-hydroxymethylpyrrolidine-3,4-diol (6s). To a solution of azidohexylpyrrolidine **5** (65 mg, 0.19 mmol) in DMF:H_2O (9:1, 2 mL), 1-ethynyl-3,5-dimethoxybenzene (43 mg, 0.26 mmol), sodium ascorbate (6 mg, 0.03 mmol) and $CuSO_4 \cdot 5H_2O$ (2.4 mg, 0.015 mmol) were added and the solution was stirred at r.t. for 24 h. After the solvent was removed under reduced pressure, the crude product was purified by chromatography column on silica gel (CH_2Cl_2:MeOH, 10:1) obtaining the final product **6s** (52.3 mg, 0.106 mmol, 56%) as a colourless oil. $[\alpha]_D^{24}$ −30.4 (*c* 0.87, MeOH). ^{1}H NMR (300 MHz, CD$_3$OD, δ ppm, *J* Hz) δ 8.32 (s, 1H, *H* triazol), 6.99 (d, 2H, $J_{H,H}$ = 2.3, Ph), 6.46 (t, 1H, Ph), 4.41 (t, 2H, $J_{H,H}$ = 7.1, -C*H$_2$*-triazole), 3.96 (t, 1H, $J_{H,H}$ = 2.0, H-3 or H-4), 3.81 (s, 6H, -OC*H$_3$*), 3.79–3.77 (m, 1H, H-4 or H-3), 3.75–3.72 (m, 1H, -C*H$_2$*OH), 3.66 (dd, 1H, $^2J_{H,H}$ = 11.3, $J_{H,5}$ = 3.4, -C*H$_2$*OH), 3.49 (dd, 1H, $^2J_{H,H}$ = 13.6, $J_{H,2}$ = 3.2, -C*H$_2$*NHAc), 3.18 (dd, 1H, $J_{H,2}$ = 7.0, -C*H$_2$*NHAc), 3.06–3.00 (m, 2H, H-2, H-5), 2.79–2.59 (m, 2H, -C*H$_2$*N-), 1.99–1.94 (m, 5H, -C*H$_2$*C*H$_2$*-triazole, -C*H$_3$*), 1.56–1.36 (m, 6H, -C*H$_2$*C*H$_2$*C*H$_2$*N-). ^{13}C NMR (75.4 MHz, CD$_3$OD, δ ppm) δ 173.5 (-*C*=O), 162.8 (Cq Ph), 148.7 (triazole), 122.5 (*C*H triazole), 133.4 (Cq Ph), 104.6 (*C* Ph), 101.3 (*C* Ph), 81.0, 80.9 (C-3, C-4), 70.3, 69.2 (C-2, C-5), 60.6 (-C*H$_2$*OH), 55.9 (-O*C*H$_3$), 51.4 (-*C*H$_2$*-triazole), 47.8 (-*C*H$_2$*N-), 39.3 (-*C*H$_2$*NHAc), 31.2 (-*C*H$_2$*C*H$_2$-triazole), 28.8, 27.7, 27.3 (-*C*H$_2$*C*H$_2$*C*H$_2$*N-), 22.7 (-*C*H$_3$). HRESIMS *m/z* found 492.2807, calc. for $C_{24}H_{38}O_6N_5$ [M+H]$^+$: 492.2817.

(2R,3R,4R,5R)-2-Acetamidomethyl-5-(hydroxymethyl)-1-(6-(4-(methoxymethyl)-1H-1,2,3-triazol-1-yl)hexyl)pyrrolidine-3,4-diol (6t). To a solution of azidohexylpyrrolidine **5** (45.7 mg, 0.14 mmol) in DMF:H_2O (9:1, 2 mL), methyl propargyl ether (16 μL, 0.18 mmol), sodium ascorbate (4 mg, 0.02 mmol) and $CuSO_4 \cdot 5H_2O$ (2 mg, 0.01 mmol) were added and the solution was stirred at r.t. for 19 h. After the solvent was removed under reduced pressure, the crude product was purified by chromatography column on silica gel (CH_2Cl_2:MeOH, 10:1 → 5:1) obtaining the final product **6t** (34 mg, 0.085 mmol, 61%) as a yellow oil. $[\alpha]_D^{25}$ −32.4 (*c* 0.83, MeOH). ^{1}H NMR (300 MHz, CD$_3$OD, δ ppm, *J* Hz) δ 7.98 (s, 1H, *H* triazol), 4.53 (s, 2H, -C*H$_2$*OCH$_3$), 4.41 (t, 2H, $J_{H,H}$ = 7.1, -C*H$_2$*-triazole), 3.96 (t, 1H, $J_{H,H}$ = 2.0, H-3 or H-4), 3.80–3.72 (m, 2H, H-

4 or H-3, -C*H$_2$*OH), 3.67 (dd, 1H, $^2J_{H,H}$ = 11.4, $J_{H,5}$ = 3.5, -C*H$_2$*OH), 3.50 (dd, 1H, $^2J_{H,H}$ = 13.6, $J_{H,2}$ = 3.2, -C*H$_2$*NHAc), 3.37 (s, 3H, -OC*H$_3$*), 3.19 (dd, 1H, $J_{H,2}$ = 6.9, -C*H$_2$*NHAc), 3.07–3.01 (m, 2H, H-2, H-5), 2.81–2.62 (m, 2H, -C*H$_2$*N-), 1.97–1.88 (m, 5H, -C*H$_2$*C*H$_2$*-triazole, -C*H$_3$*), 1.59–1.34 (m, 6H, -C*H$_2$*C*H$_2$*C*H$_2$*N-). ^{13}C NMR (75.4 MHz, CD$_3$OD, δ ppm) δ 173.6 (-*C*=O), 145.8 (Cq triazole), 125.0 (*C*H triazole), 81.0, 80.9 (C-3, C-4), 70.4, 69.3 (C-2, C-5), 66.3 (-*C*H$_2$*OCH$_3$), 60.6 (-*C*H$_2$*OH), 58.4 (-O*C*H$_3$), 51.3 (-*C*H$_2$*-triazole), 47.8 (-*C*H$_2$*N-), 39.3 (-*C*H$_2$*NHAc), 31.2 (-*C*H$_2$*C*H$_2$-triazole), 28.8, 27.7, 27.2 (-*C*H$_2$*C*H$_2$*C*H$_2$*N-), 22.7 (-*C*H$_3$). HRESIMS *m/z* found 400.2546, calc. for $C_{18}H_{34}O_5N_5$ [M+H]$^+$: 400.2554.

(2R,3R,4R,5R)-2-Acetamidomethyl-5-(hydroxymethyl)-1-(6-(3-phenylthioureido)hexyl)pyrrolidine-3,4-diol (7A). To a solution of aminohexylpyrrolidine **3b** [30] (30 mg, 0.099 mmol) in MeOH (2 mL), phenyl isothiocyanate (15 μL, 0.12 mmol) was added and the mixture was stirred for 5 h at r.t. After evaporation to dryness, the crude product was purified by chromatography column on silica gel (EtOAc:MeOH, 5:1) to give **7A** (27 mg, 0.062 mmol, 63%) as a yellow oil. $[\alpha]_D^{24}$ −36.7 (*c* 0.72, MeOH). ^{1}H NMR (300 MHz, CD$_3$OD, δ ppm, *J* Hz) δ 7.40–7.30 (m, 4H, Ph), 7.23–7.17 (m, 1H, Ph), 3.97 (t, 1H, $J_{H,H}$ = 2.1, H-3 or H-4), 3.80–3.75 (m, 2H, H-4 or H-3, -C*H$_2$*OH), 3.69 (dd, 1H, $^2J_{H,H}$ = 11.4, $J_{H,5}$ = 3.5, -C*H$_2$*OH), 3.58–3.48 (m, 3H, -C*H$_2$*NH-, -C*H$_2$*NHAc), 3.22 (dd, 1H, $^2J_{H,H}$ = 13.6, $J_{H,2}$ = 6.9, -C*H$_2$*NHAc), 3.09–3.03 (m, 2H, H-2, H-5), 2.84–2.65 (m, 2H, -C*H$_2$*N-), 1.95 (s, 3H, -C*H$_3$*), 1.65–1.58 (m, 4H, -C*H$_2$*C*H$_2$*N-, -C*H$_2$*C*H$_2$*NH-), 1.41–1.36 (m, 4H, -C*H$_2$*C*H$_2$). ^{13}C NMR (75.4 MHz, CD$_3$OD, δ ppm) δ 182.0 (-*C*=S), 173.6 (-*C*=O), 130.3–125.7 (Cq Ph, C Ph), 81.0, 80.8 (C-3, C-4), 70.4, 69.4 (C-2, C-5), 60.6 (-*C*H$_2$*OH), 48.0 (-*C*H$_2$*N-), 45.7 (-*C*H$_2$*NH-), 39.3 (-*C*H$_2$*NHAc), 30.0, 29.0 (-*C*H$_2$*C*H$_2$*N-, -*C*H$_2$*C*H$_2$*NH-), 28.1, 27.7 (-*C*H$_2$*C*H$_2$), 22.7 (-*C*H$_3$). HRESIMS *m/z* found 439.2366, calc. for $C_{21}H_{35}O_4N_4S$ [M+H]$^+$: 439.2374.

(2R,3R,4R,5R)-2-Acetamidomethyl-5-hydroxymethyl-1-(6-(3-(3,5-bis(trifluoromethyl)phenyl)thioureido)hexyl)pyrrolidine-3,4-diol (7D). To a solution of aminohexylpyrrolidine **3b** [30] (45 mg, 0.15 mmol) in MeOH (3 mL) we added 3,5-bis(trifluoromethyl)phenyl isothiocyanate (30 μL, 0.18 mmol) and the mixture was stirred for 24 h at r.t. After evaporation to dryness, the crude product was purified by chromatography column on silica gel (EtOAc:MeOH, 10:1) to give **7D** (45 mg, 0.078 mmol, 52%) as a colorless oil. $[\alpha]_D^{24}$ −30.2 (*c* 0.92, MeOH). ^{1}H NMR (300 MHz, CD$_3$OD, δ ppm, *J* Hz) δ 8.18 (s, 2H, Ph), 7.62 (s, 1H, Ph), 3.97 (t, 1H, $J_{H,H}$ = 2.0, H-3 or H-4), 3.80–3.75 (m, 2H, H-4 or H-3, -C*H$_2$*OH), 3.68 (dd, 1H, $^2J_{H,H}$ = 11.3, $J_{H,5}$ = 3.3, -C*H$_2$*OH), 3.61–3.57 (m, 2H, -C*H$_2$*NH-), 3.51 (dd, 1H, $^2J_{H,H}$ = 13.6, $J_{H,2}$ = 3.2, -C*H$_2$*NHAc), 3.20 (dd, 1H, $J_{H,2}$ = 7.0, -C*H$_2$*NHAc), 3.07–3.01 (m, 2H, H-2, H-5), 2.83–2.63 (m, 2H, -C*H$_2$*N-), 1.96 (s, 3H, -C*H$_3$*), 1.69–1.60 (m, 4H, -C*H$_2$*C*H$_2$*N-, -C*H$_2$*C*H$_2$*NH-), 1.43–1.41 (m, 4H, -C*H$_2$*C*H$_2$). ^{13}C NMR (75.4 MHz, CD$_3$OD, δ ppm, *J* Hz) δ 182.6 (-*C*=S), 173.5 (-*C*=O), 143.2 (Cq Ph), 132.6 (q, $^2J_{C,F}$ = 33.1, Cq Ph), 124.7 (q, $^1J_{C,F}$ = 271.6, -C*F$_3$*), 123.7–122.9 (m, C Ph), 117.8–117.5 (m, C Ph), 81.1, 80.9 (C-3, C-4), 70.3, 69.2 (C-2, C-5), 60.7 (-*C*H$_2$*OH), 47.8 (-*C*H$_2$*N-), 45.4 (-*C*H$_2$*NH-), 39.4 (-*C*H$_2$*NHAc), 29.7, 29.1 (-*C*H$_2$*C*H$_2$*N-, -*C*H$_2$*C*H$_2$*NH-), 28.1, 27.8 (-*C*H$_2$*C*H$_2$), 22.7 (-*C*H$_3$). HRESIMS *m/z* found 575.2112, calc. for $C_{23}H_{33}O_4N_4F_6S$ [M+H]$^+$: 575.2121.

Dimer 8a. Azidohexylpyrrolidine **5** (43 mg, 0.13 mmol) was added to a solution of the dialkyne **a** (15 mg, 0.054 mmol) in *t*-BuOH:H_2O (4:1, 2.6 mL) followed by sodium ascorbate (10 mg, 0.050 mmol) and $CuSO_4 \cdot 5H_2O$ (2.4 mg, 0.015 mmol) and the reaction mixture was heated at 80 °C for 24 h. After the solvent was removed under vacuum, the crude product was purified by chromatography column on silica gel (DCM:MeOH:NH$_4$OH, 3:1:0.05 → 3:1:0.1) obtaining the final product **8a** (26 mg, 0.028 mmol, 52%) as a yellow solid. $[\alpha]_D^{29}$-17.5 (*c* 0.86, MeOH). ^{1}H NMR (300 MHz, CD$_3$OD, δ ppm, *J* Hz) δ 7.98 (s, 2H, *H* triazole), 4.62 s, 4H, triazole-C*H$_2$*-O-), 4.40 (t, 4H, $J_{H,H}$ = 7.0, -C*H$_2$*-triazole), 3.98 (br. t, $J_{H,H}$ = 2.0, H-3 or H-4), 3.82 (br. t, 2H, H-4 or H-3), 3.77 (dd, 2H, $^2J_{H,H}$ = 11.5, $J_{H,5}$ = 4.8, -C*H$_2$*OH), 3.69 (dd, 2H, $J_{H,5}$ = 3.7, -C*H$_2$*OH), 3.67–3.62 (m, 16H, -OC*H$_2$*C*H$_2$*O-), 3.51 (dd, 2H, $^2J_{H,H}$ = 13.7, $J_{H,2}$ = 3.4, -C*H$_2$*NHAc), 3.24 (dd, 2H, $J_{H,2}$ = 6.9, -C*H$_2$*NHAc), 3.10–3.05 (m, 4H, H-

2, H-5), 2.86–2.68 (m, 4H, -CH_2N-), 1.95–1.87 (m, 10*H*, -CH_2CH_2-triazole, -CH_3), 1.59–1.31 (m, 12H, CH_2CH_2CH_2N-). ^{13}C NMR (75.4 MHz, CD$_3$OD, δ ppm) δ 173.7 (-*C*=O), 145.9 (Cq triazole), 125.0 (*C*H triazole), 80.7, 80.6 (C-3, C-4), 71.5, 71.4 (-O*C*H$_2$CH$_2$O-), 70.7, 69.9 (C-2, C-5), 65.0 (triazole-*C*H$_2$-O-), 60.5 (-*C*H$_2$OH), 51.3 (-*C*H$_2$-triazole), 48.2 (-*C*H$_2$N-), 39.2 (-*C*H$_2$NHAc), 31.2 (-*C*H$_2$CH$_2$-triazole), 28.6, 27.7, 27.2 (-*C*H$_2$CH$_2$CH$_2$N-), 22.7 (-*C*H$_3$). HRESIMS *m/z* found 951.5477, calc. for C$_{42}$H$_{76}$O$_{13}$N$_{10}$ [M+Na]$^+$: 951.5486.

Dimer 9D. Pyrrolidine-amine **3b** [30] (30 mg, 0.099 mmol) was added to a solution of the diisothiocyanate **D** (14 mg, 0.042 mmol) in DCM:MeOH 1:10 (2.3 mL) and the mixture was stirred for 24 h at r.t. After evaporation to dryness, the crude was purified by chromatography column on silica gel (DCM:MeOH:NH$_4$OH, 3:1:0.03) obtaining the final product **9D** (32 mg, 0.034 mmol, 81%) as a white solid. $[\alpha]_D^{29}$-21.0 (c 0.88, MeOH). ^{1}H NMR (300 MHz, CD$_3$OD, δ ppm, *J* Hz) δ 7.85 (d, 4H, *J*$_{H,}$ $_H$ = 8.8, Ph), 7.70 (d, 4H, Ph), 3.99–3.96 (m, 2H, H-3 or H-4), 3.83–3.76 (m, 4H, H-4 or H-3, -CH_2OH), 3.70 (dd, 2H, $^2J_{H,H}$ = 11.5, *J*$_{H,5}$ = 3.6, -CH_2OH), 3.57–3.49 (m, 6H, -CH_2NH-, -CH_2NHAc), 3.25 (dd, 2H, $^2J_{H,H}$ = 13.7, *J*$_{H,2}$ = 6.8, -CH_2NHAc), 3.14–3.08 (m, 4H, H-2, H-5), 2.87–2.70 (m, 4H, -CH_2N-), 1.95 (s, 6H, -CH_3), 1.65–1.58 (m, 8H, -CH_2CH_2N-, -CH_2CH_2NH-), 1.43–1.33 (m, 8H, -CH_2CH_2). ^{13}C NMR (75.4 MHz, CD$_3$OD, δ ppm) δ 182.0 (-*C*=S), 173.8 (-*C*=O), 145.6 (Cq Ph), 137.3 (Cq Ph), 129.4 (Ph), 123.2 (Ph), 80.7, 80.6 (C-3, C-4), 70.6, 69.6 (C-2, C-5), 60.5 (-*C*H$_2$OH), 48.3 (-*C*H$_2$N-), 45.5 (-*C*H$_2$NH-), 39.2 (-*C*H$_2$NHAc), 29.7, 28.7 (-*C*H$_2$CH$_2$N-, -*C*H$_2$CH$_2$NH-), 28.0, 27.7 (-*C*H$_2$CH$_2$), 22.7 (-*C*H$_3$). HRESIMS *m/z* found 939.4127, calc. for C$_{42}$H$_{66}$O$_{10}$N$_8$S$_3$ [M+H]+: 939.4128.

Declaration of Competing Interest

The authors declare that they have no known competing financial interests or personal relationships that could have appeared to influence the work reported in this paper.

Acknowledgements

Appendix A. Supplementary material

Supplementary data to this article can be found online at https://doi.org/10.1016/j.bioorg.2022.105650.

References

[1] (a) K. Slámová, P. Bojarová, L. Petrásková, V. Křen, β-N-Acetylhexosaminidase: what's in a name…? Biotechnol. Adv. 28 (2010) 682–693;
(b) K. Slámová, P. Bojarová, Engineered N-acetylhexosamine-active enzymes in glycoscience, BBA 1861 (2017) 2070–2087.

[2] T. Liu, J. Yan, Q. Yang, Comparative biochemistry of GH3, GH20 and GH84 β-*N*-acetyl-D-hexosaminidases and recent progress in selective inhibitor discover, Curr. Drug Targets 13 (2012) 512–525.

[3] F. Zhou, J. Huo, Y. Liu, H. Liu, G. Liu, Y. Chen, B. Chen, Elevated glucose levels impair the WNT/ β-catenin pathway *via* the activation of the hexosamine biosynthesis pathway in endometrial cancer, J. Steroid Biochem. 159 (2016) 19–25.

[4] A.R. Shikhman, D.C. Brinson, M. Lotz, Profile of glycosaminoglycan-degrading glycosidases and glycoside sulfatases secreted by human articular chondrocytes in homeostasis and inflammation, Arthritis Rheum. 43 (2000) 1307–1314.

[5] For a recent review on this enzyme: T. Liu, Y. Duan, Q. Yang, Revisiting glycoside hydrolase family 20 β-*N*-acetyl-D-hexosaminidases: crystal structures, physiological substrates and specific inhibitors Biotechnol. Adv. 36 (2018) 1127–1138.

[6] A.A. Elbatrawy, E.J. Kim, G. Nam, *O*-GlcNAcase: emerging mechanism, substrate recognition and small-molecule inhibitors, ChemMedChem 15 (14) (2020) 1244–1257.

[7] F.M. Platt, Sphingolipid lysosomal storage disorders, Nature 510 (7503) (2014) 68–75.

[8] J.-Q. Fan, A contradictory treatment for lysosomal storage disorders: inhibitors enhance mutant enzyme activity, Trends Pharmacol. Sci. 24 (7) (2003) 355–360.

[9] E.M. Sánchez-Fernández, J.M. García Fernández, C.O. Mellet, Glycomimetic-based pharmacological chaperones for lysosomal storage disorders: lessons from Gaucher, GM1-gangliosidosis and Fabry diseases, Chem. Commun. 52 (32) (2016) 5497–5515.

[10] For examples of pharmacological chaperones for Tay-Sachs and/or Sandhoff disease, see: (a) M.B. Tropak, J.E. Blanchard, S.G. Withers, E.D. Brown, D. Mahuran, High-throughput screening for human lysosomal β-*N*-acetyl hexosaminidase inhibitors acting as pharmacological chaperones, Chem. Biol. 14 (2007) 153–164;
(b) M.B. Tropak, S.P. Reid, M. Guiral, S.G. Withers, D. Mahuran, Pharmacological enhancement of β-hexosaminidase activity in fibroblasts from adult Tay-Sachs and Sandhoff patients, J. Biol. Chem. 279 (2004) 13478–13487;
(c) A. Kato, I. Nakagome, S. Nakagawa, K. Kinami, I. Adachi, S.F. Jenkinson, J. Désiré, Y. Blériot, R.J. Nash, G.W.J. Fleet, S. Shuichi Hirono, *In silico* analyses of essential interactions of iminosugars with the Hex A active site and evaluation of their pharmacological chaperone effects for Tay-Sachs disease, Org. Biomol. Chem. 15 (2017) 9297–9304;
(d) A. De la Fuente, R. Rísquez-Cuadro, X. Verdaguer, J.M. García Fernández, E. Nanba, K. Higaki, C. Ortiz Mellet, A. Riera, Efficient stereoselective synthesis of 2-acetamido-1,2-dideoxyallonojirimycin (DAJNAc) and sp^2-iminosugar conjugates: Novel hexosaminidase inhibitors with discrimination capabilities between the mature and precursor forms of the enzyme, Eur. J. Med. Chem. 121 (2016) 926–938.

[11] a) A.R. Shikhman, D.C. Brinson, M. Lotz, Profile of glycosaminoglycan-degrading glycosidases and glycoside sulfatases secreted by human articular chondrocytes in homeostasis and inflammation, Arthritis Rheum. 43 (2000) 1307–1314;
b) M. Pásztói, G. Nagy, P. Géher, T. Lakatos, K. Tóth, K. Wellinger, P. Pócza, B. György, M.C. Holub, A. Kittel, K. Pálóczy, M. Mazán, P. Nyirkos, A. Falus, E. I. Buzas, Gene expression and activity of cartilage degrading glycosidases in human rheumatoid arthritis and osteoarthritis synovial fibroblasts, Arthritis Res. Ther. 11 (2009) R68.

[12] J. Liu, A.R. Shikhman, M.K. Lotz, C.-H. Wong, Hexosaminidase inhibitors as new drug candidates for the therapy of osteoarthritis, Chem. Biol. 8 (2001) 701–711.

[13] C. Roth, S. Chan, W.A. Offen, G.R. Hemsworth, L.I. Willems, D.T. King, V. Varghese, R. Britton, D.J. Vocadlo, G.J. Davies, Structural and functional insight into human *O*-GlcNAcase, Nat. Chem. Biol. 13 (2017) 610–612.

[14] S.A. Yuzwa, D.J. Vocadlo, *O*-GlcNAc and neurodegeneration: Biochemical mechanisms and potential roles in Alzheimer's disease and beyond, Chem. Soc. Rev. 43 (2014) 6839–6858.

[15] C.M. Ferrer, M.J. Reginato, Sweet connections: *O*-GlcNAcylation links cancer cell metabolism and survival, Mol. Cell Oncol. 2 (2014) 961809.

[16] S. Gerber-Lemaire, F. Popowycz, E. Rodríguez-García, A.T. Carmona-Asenjo, I. Robina, P. Vogel, An efficient combinatorial method for the discovery of glycosidase inhibitors, ChemBioChem 5 (2002) 466–470.

[17] P. Elías-Rodríguez, E. Moreno-Clavijo, A.T. Carmona, A.J. Moreno-Vargas, I. Robina, Rapid discovery of potent α-fucosidase inhibitors by *in situ* screening of a library of (pyrrolidin-2-yl)triazoles, Org. Biomol. Chem. 12 (31) (2014) 5898–5904.

[18] (a) M. Martínez-Bailén, A.T. Carmona, E. Moreno-Clavijo, I. Robina, D. Ide, A. Kato, A.J. Moreno-Vargas, Tuning of β-glucosidase and α-galactosidase inhibition by generation and in situ screening of a library of pyrrolidine-triazole hybrid molecules, Eur. J. Med. Chem. 138 (2017) 532–542;
(b) P. Elías-Rodríguez, V. Pingitore, A.T. Carmona, A.J. Moreno-Vargas, D. Ide, S. Miyawaki, A. Kato, E. Álvarez, I. Robina, Discovery of a potent α–galactosidase inhibitor by in situ analysis of a library of pyrrolizidine-(thio)urea hybrid molecules generated via click chemistry, J. Org. Chem. 83 (2018) 8863–8873.

[19] A.T. Carmona, S. Carrión-Jiménez, V. Pingitore, E. Moreno-Clavijo, I. Robina, A. J. Moreno-Vargas, Harnessing pyrrolidine iminosugars into dimeric structures for the rapid discovery of divalent glycosidase inhibitors, Eur. J. Med. Chem. 151 (2018) 765–776.

[20] (a) C. Müller, G. Despras, T.K. Lindhorst, Organizing multivalency in carbohydrate recognition, Chem. Soc. Rev. 45 (2016) 3275–3302;
(b) M. González-Cuesta, C. Ortiz Mellet, J.M. García-Fernández, Carbohydrate supramolecular chemistry: beyond the multivalent effect, Chem. Commun. 56 (2020) 5207–5222.

[21] For reviews, see: (a) P. Compain, A. Bodlenner, The multivalent effect in glycosidase inhibition: a new, rapidly emerging topic in glycoscience, ChemBioChem 15 (2014) 1239–1251;
(b) S.G. Gouin, Multivalent inhibitors for carbohydrate-processing enzymes: beyond the "lock-and-key" concept, Chem. Eur. J. 20 (2014) 11616–11628;
(c) R. Zelli, J.-F. Longevial, P. Dumy, A. Marra, Synthesis and biological properties of multivalent iminosugars, New J. Chem. 30 (2015) 5050–5074;
(c) C. Matassini, C. Parmeggiani, F. Cardona, A. Goti, Are enzymes sensitive to the multivalent effect? Emerging evidence with glycosidases. Tetrahedron Lett. 57 (2016) 5407–5415.

[22] P. Compain, Multivalent effect in glycosidase inhibition: the end of the beginning, Chem. Rec. 20 (2020) 10–22.

[23] S. Mirabella, G. D'Adamio, C. Matassini, A. Goti, S. Delgado, A. Gimeno, I. Robina, A.J. Moreno-Vargas, S. Sestak, J. Jiménez-Barbero, F. Cardona, Mechanistic insight into the binding of multivalent pyrrolidine to α-mannosidases, Chem. Eur. J. 23 (2017) 14585–14596.

[24] J.-F. Nierengarten, J.P. Schneider, T.M.N. Trinh, A. Joosten, M. Holler, M. L. Lepage, A. Bodlenner, M.I. García-Moreno, C. Ortiz Mellet, P. Compain, Giant glycosidase inhibitors: first- and second-generation fullerodendrimers with a dense iminosugar shell, Chem. Eur. J. 24 (2018) 2483–2492.

[25] (a) G. D'Adamio, C. Matassini, C. Parmeggiani, S. Catarzi, A. Morrone, A. Goti, P. Paoli, F. Cardona, Evidence for a multivalent effect in inhibition of sulfatases involved in lysosomal storage disorders (LSDs), RSC Adv. 6 (2016) 64847–64851;
(b) C. Matassini, C. Vanni, A. Goti, A. Morrone, M. Marradi, F. Cardona, Multimerization of DAB-1 onto Au GNPs affords new potent and selective N-acetylgalactosamine-6-sulfatase (GALNS) inhibitors, Org. Biomol. Chem. 16 (2018) 8604–8612.

[26] M. Martínez-Bailén, A.T. Carmona, F. Cardona, C. Matassini, A. Goti, M. Kubo, A. Kato, I. Robina, A.J. Moreno-Vargas, Synthesis of multimeric pyrrolidine iminosugar inhibitors of human β-glucocerebrosidase and α-galactosidase A: First example of a multivalent enzyme activity enhancer for Fabry disease, Eur. J. Med. Chem. 192 (2020) 112173.

[27] Selected references: (a) K.A. Stubbs, M.S. Macauley, D.J. Vocadlo, A selective inhibitor Gal-PUGNAc of human lysosomal β-hexosaminidases modulates levels of the ganglioside GM2 in neuroblastoma cells, Angew. Chem. Int. Ed. 48 (2009) 1300–1303;
(b) C.W. Ho, S.D. Popat, T.-W. Liu, K.-C. Tsai, M.-J. Ho, W.-H. Chen, A.-S. Yang, C.-H. Lin, Development of GlcNAc-inspired iminocyclitols as potent and selective N-acetyl-β-hexosaminidase inhibitors, ACS Chem. Biol. 5 (2010) 489–497;
(c) M. Bergeron-Brlek, J. Goodwin-Tindall, N. Cekic, C. Roth, W.F. Zandberg, X. Shan, V. Varghese, S. Chan, G.J. Davies, D.J. Vocadlo, R. Britton, A convenient approach to stereoisomeric iminocyclitols: generation of potent brain-permeable OGA inhibitors, Angew. Chem. Int. Ed. 54 (2015) 15429–15433;
(d) S. Shen, L. Dong, W. Chen, X. Zeng, H. Lu, Q. Yang, J. Zhang, Modification of the thioglycosyl–naphthalimides as potent and selective human O-GlcNAcase inhibitors, ACS Med. Chem. Lett. 9 (2018) 1241–1246;
(e) P. Weber, S.A. Nasseri, B.M. Pabst, A. Torvisco, P. Müller, E. Paschke, M. Tschernutter, W. Windischhofer, S.G. Withers, T.M. Wrodnigg, A.E. Stütz, Potent GH20 N-Acetyl-β-D-hexosaminidase inhibitors: N-substituted 3-acetamido-4-amino-5-hydroxymethyl-cyclopentanediols, Molecules 23 (2018) 708.

[28] D. Alvárez-Dorta, D.T. King, T. Legigan, D. Ide, I. Adachi, D. Deniaud, J. Desire, A. Kato, D. Vocadlo, S.G. Gouin, Y. Bleriot, Multivalency to inhibit and discriminate hexosaminidases, Chem. Eur. J. 23 (2017) 9022–9025.

[29] J. Liu, M.M.D. Numa, H. Liu, S.-J. Huang, P. Sears, A.R. Shikhman, C.-H. Wong, Synthesis and high-throughput screening of N-acetyl-β-hexosaminidase inhibitor libraries targeting osteoarthritis, J. Org. Chem. 69 (2004) 6273–6283.

[30] P.-H. Liang, W.-C. Cheng, Y.-L. Lee, H.-P. Yu, Y.T. Wu, Y.-L. Lin, C.-H. Wong, Novel five-membered iminocyclitol derivatives as selective and potent glycosidase inhibitors: new structures for antivirals and osteoarthritis, ChemBioChem 7 (2006) 165–173.

[31] M.B. Tropak, J.E. Blanchard, S.G. Withers, E.D. Brown, D. Mahuran, High-throughput screening for human lysosomal β-N-acetyl hexosaminidase inhibitors acting as pharmacological chaperones, Chem. Biol. 14 (2007) 153–164.

[32] J. Krejzová, N. Kulik, K. Slámová, V. Křen, Expression of human β-N-acetylhexosaminidase B eases the search for selective inhibitors, Enzyme Microb. Technol. 89 (2016) 1–6.

[33] B.L. Mark, D.J. Mahuran, M.M. Cherney, D. Zhao, S. Knapp, M.N. James, Crystal structure of human beta-hexosaminidase B: understanding the molecular basis of Sandhoff and Tay-Sachs disease, J. Mol. Biol. 327 (2003) 1093–1109.

[34] T. Maier, N. Strater, C.G. Schuette, R. Klingenstein, K. Sandhoff, W. Saenger, The X-ray crystal structure of human beta-hexosaminidase B provides new insights into Sandhoff disease, J. Mol. Biol. 328 (2003) 669–681.

[35] H. Land, M.S. Humble, YASARA: A tool to obtain structural guidance in biocatalytic investigations, Methods in Molecular Biology vol. 1685 (2018) 43–67.

[36] R.A. Friesner, J.L. Banks, R.B. Murphy, T.A. Halgren, J.J. Klicic, D.T. Mainz, M. P. Repasky, E.H. Knoll, D.E. Shaw, M. Shelley, J.K. Perry, P. Francis, P.S. Shenkin, Glide: a new approach for rapid, accurate docking and scoring. 1. Method and assessment of docking accuracy, J. Med. Chem. 47 (2004) 1739–1749.

[37] R.A. Friesner, R.B. Murphy, M.P. Repasky, L.L. Frye, J.R. Greenwood, T.A. Halgren, P.C. Sanschagrin, D.T. Mainz, Extra precision glide: docking and scoring incorporating a model of hydrophobic enclosure for protein-ligand complexes, J. Med. Chem. 49 (2006) 6177–6196.

[38] J. Du, H. Sun, L. Xi, J. Li, Y. Yang, H. Liu, X. Yao, Molecular modeling study of checkpoint kinase 1 inhibitors by multiple docking strategies and prime/MM-GBSA calculation, J. Comput. Chem. 32 (2011) 2800–2809.

[39] M.F. Adasme, K.L. Linnemann, S.N. Bolz, F. Kaiser, S. Salentin, V.J. Haupt, M. Schroeder, PLIP 2021: expanding the scope of the protein–ligand interaction profiler to DNA and RNA, Nucleic Acids Res. 49 (2021) W530–W534.

[40] A.C. Wallace, R.A. Laskowski, J.M. Thornton, LIGPLOT: a program to generate schematic diagrams of protein-ligand interactions, Protein Eng. Des. Sel. 8 (1995) 127–134.

[41] M.J. Frisch, G.W. Trucks, H.B. Schlegel, G.E. Scuseria, M.A. Robb, J.R. Cheeseman, G. Scalmani, V. Barone, G.A. Petersson, H. Nakatsuji, X. Li, M. Caricato, A. Marenich, J. Bloino, B.G. Janesko, R. Gomperts, B. Mennucci, H.P. Hratchian, J. V. Ortiz, A.F. Izmaylov, J.L. Sonnenberg, D. Williams-Young, F. Ding, F. Lipparini, F. Egidi, J. Goings, B. Peng, A. Petrone, T. Henderson, D. Ranasinghe, V. G. Zakrzewski, J. Gao, N. Rega, G. Zheng, W. Liang, M. Hada, M. Ehara, K. Toyota, R. Fukuda, J. Hasegawa, M. Ishida, T. Nakajima, Y. Honda, O. Kitao, H. Nakai, T. Vreven, K. Throssell, J.A. Montgomery Jr., J.E. Peralta, F. Ogliaro, M. Bearpark, J.J. Heyd, E. Brothers, K.N. Kudin, V.N. Staroverov, T. Keith, R. Kobayashi, J. Normand, K. Raghavachari, A. Rendell, J.C. Burant, S.S. Iyengar, J. Tomasi, M. Cossi, J.M. Millam, M. Klene, C. Adamo, R. Cammi, J.W. Ochterski, R.L. Martin, K. Morokuma, O. Farkas, J.B. Foresman, D.J. Fox, Gaussian 09, Revision A.02, Gaussian, Inc., Wallingford CT, 2016.

[42] H.M. Berman, T. Battistuz, T.N. Bhat, W.F. Bluhm, P.E. Bourne, K. Burkhardt, Z. Feng, G.L. Gilliland, L. Iype, S. Jain, P. Fagan, J. Marvin, D. Padilla, V. Ravichandran, B. Schneider, N. Thanki, H. Weissig, J.D. Westbrook, C. Zardecki, The protein data bank, Acta Crystallogr. D Biol. Crystallogr. 58 (2002) 899–907.

[43] X. Xu, W.A. Goddard, The X3LYP extended density functional for accurate descriptions of nonbond interactions, spin states, and thermochemical properties, PNAS 101 (2004) 2673–2677.

[44] P.R. Varadwaj, A. Varadwaj, H.M. Marques, Halogen bonding: a halogen-centered noncovalent interaction yet to be understood, Inorganics 7 (2019) 40.